Supplementary Information (SI) for Environmental Science: Nano.

Supplementary Information

Efficient peroxydisulfate activation by CoNiFc-MOF for rapid removal of emerging contaminants via both radical and non-radical pathways

Maierhaba·Kuerban[1], Yun Wang[1], Dilnur Dilxat[1], Nuzahat Habibul[1*], Yanyun Hu[*2]

1. *College of Chemistry and Chemical Engineering, Xinjiang Normal University, Urumqi 830054, China*
2. *University of Science and Technology of China, Hefei, 230026, China*

*** Corresponding author.**

E-mail addresses: nuzahat@mail.ustc.edu.cn (N. Habibul); yanyunhu@ustc.edu.cn

Table of Contents

Part S1. Supplementary Texts

Part S2. Supplementary Figures

Fig. S9. (a) XPS survey of CoNiFc-MOF. High resolution XPS spectra of (b) Co 2p, (c) Fe 2p, (d) Ni 2p of catalysts.

Fig. S10. Adsorption of BPA by NiFc-MOF, CoFc-MOF and CoNiFc-MOF catalysts.

Fig. S11. Effects of different BPA concentrations on degradation.

Fig. S12. Effect of different temperatures on BPA removal.

Fig. S13. Premixing CoNiFc-MOF and PDS on BPA degradation.

Fig. S14. BPA degradation in CoNiFc-MOF/PDS system with or without N_2 bubbling.

Fig. S15. (a) PMSO consumption and $PMSO_2$ generation in in different systems: CoNiFc-MOF alone system. (b) CoNiFc-MOF/PDS system.

Fig. S16. Effect of DMSO on BPA degradation in the CoNiFc-MOF/PDS system.

Fig. S17. ROS contribution of CoNiFc-MOF/PDS system.

Fig. S18. (a) Electrochemical impedance spectroscopy (EIS) analysis of CoNiFc-MOF, CoFc-MOF and NiFc-MOF samples; (b) LSV results of CoNiFc-MOF, CoFc-MOF and NiFc-MOF.

Fig. S19 MS spectra of the BPA intermediates detected in the CoNiFc-MOF/PDS system.

Part S3. Supplementary Tables

Table S1. The HPLC analysis conditions for different organic compounds.

Table S2. Relative element content (wt.%) on catalyst surface.

Table S3. The changes in the content of elemental valence states before and after the CoNiFc-MOF reaction.

Table S4. The identified intermediates of BPA by UPLC-Q-TOF-MS in the CoNiFc-MOF/PDS system.

Table S5. Calculate the percentage ratio of different metals leaching

Table S6. The comparison of recently reported transition metal catalysts in PMS/PDS activation for the removal of BPA.

Part S1. Supplementary Texts

Text S1. Chemicals and reagents

1,1′-ferrocene dicarboxylate acid (98%), bisphenol A (BPA), bisphenol B (BPB), Methyl phenyl sulfoxide (PMSO), methyl phenyl sulfone ($PMSO_2$), oxytetracycline (OTC), tetracycline (TC), phenol (PE), L-Histidine and dimethyl sulfoxide (DMSO) and Nafion were purchased from Macklin Co. Ethanol (EtOH), methanol (MeOH, HPLC), acetonitrile (≥99.9%, HPLC), humic acid (HA), N, N-dimethylformamide (DMF) were purchased from Sigma Aldrich Co. Nickel chloride hexahydrate ($NiCl_2 \cdot 6H_2O$), cobalt chloride hexahydrate ($CoCl_2 \cdot 6H_2O$), persulfate (PDS, $K_2S_2O_8$), sulfuric acid (H_2SO_4), potassium iodide (KI), p-benzoquinone (BQ), 5,5-dimethyl-1-pyrrolineN-oxide (DMPO), 2,2,6,6-tetramethyl-4-piperidinol (TEMP) were all provided from Aladdin. Methyl alcohol (MeOH), Tert-butyl alcohol (TBA), sodium chloride (NaCl, AR), sodium dihydrogen phosphate (NaH_2PO_4), sodium bicarbonate ($NaHCO_3$), sodium sulfate (Na_2SO_4) and Sodium hydroxide (NaOH) were purchased from Tianjin Chemical Reagent Co.

Text S2. Synthesis of CoFc-MOF and NiFc-MOF catalysts

The synthesis procedure for the CoFc-MOF catalyst as follows: Dissolve 0.5 mmol of 1,1'-ferrocene dicarboxylic acid (0.14 g) in 15 mL of DMF, and 1 mmol of $CoCl_2 \cdot 6H_2O$ (0.26 g) in 15 mL of methanol. These solutions are then combined in a 50 mL Teflon-lined stainless steel autoclave and heated at 120°C for 12 h. The resultant product was washed three times with DMF and anhydrous ethanol. Finally, the brown CoFc-MOF catalyst is obtained by drying at 60℃ for 12 h. Following extensive experimentation and measurement, the average reaction yield of the catalyst was determined to be approximately 25%.

The synthesis method for the NiFc-MOF catalyst is as follows: Dissolve 0.5 mmol of 1,1'-ferrocene dicarboxylic acid (0.14 g) in 15 mL of DMF, and dissolve 1 mmol of $NiCl_2 \cdot 6H_2O$ (0.38 g) in 15 mL of methanol. Combine these solutions in a 50 mL Teflon-lined stainless steel autoclave and heat at 120℃ for 12 h. Subsequently, wash three times with DMF and anhydrous ethanol. Finally, the dark brown NiFc-MOF catalyst can be obtained by drying at 60℃ for 12 h. The average reaction yielding an average reaction yield of approximately 20%.

The preparation parameters of the CoNiFc-MOF catalyst were optimized using a single-factor control method. By comparing the efficiency of catalysts synthesized under different conditions in activating PDS for BPA removal, the optimal synthesis conditions for the catalyst were determined. The effects of reaction temperature, reaction time, and different metal source ratios on the catalyst synthesis were initially investigated. The synthesis temperature was controlled at 90-150°C, and the reaction time was within 9-15 h. It was found that the catalytic performance of CoNiFc-MOF catalysts prepared at different reaction temperatures and times varied significantly. When the reaction temperature was 120°C and the reaction time was 12 h, the BPA removal rate was the best within 5 min (Fig. S2 (a)). Therefore, the optimal temperature and reaction time were determined to be 120°C and 12 h, respectively. Among different metal source ratios, a molar ratio of 4:1 for Co and Ni sources showed better BPA removal efficiency (Fig. S2 (b)).

Text S3. Conditions for monitoring the reaction of target pollutants by HPLC

In this study, the content of the pollutant to be measured was calculated by the external standard method. First, a series of standard solutions with different concentrations were prepared, ranging from 0.05 ~ 12 mg/L. By measuring the peak areas of the above-mentioned standard solutions with known concentrations and taking the concentration of the standard solution as the abscissa and the peak area corresponding to the pollutant to be measured as the ordinate, a standard curve was plotted. The retention time for the target pollutant BPA is 5 min. The linear equation obtained was $y=0.9225x-0.0789$, $R^2=0.9996$ (Fig.S1). The concentration of the sample can be calculated by substituting the peak area of the sample to be measured into the above equation. The concentration data of the target pollutants were obtained through multiple measurements, and the standard deviation was calculated to be 0.2294 mg/L with a relative standard deviation of 2.18%.

Text S4. Characterizations

Scanning electron microscopy (SEM, Sigma 300, Zeiss, Germany) with energy dispersive spectrometer (EDS) was employed to examine the surface morphology and elemental composition. X-ray diffractometer (XRD, Bruker-AXS, Germany) analysis was conducted with Cu Kα radiation over a 2θ range of 5-70°. Fourier transform infrared spectrometer (FTIR, Tensor27, America) was used to identify functional groups present in the sample. The N_2 adsorption/desorption isotherm was analyzed through Brunauer-Emmett-Teller theory (BET, Micromeritics ASAP 2460) to determine the surface area. The thermal stability of the catalyst was studied by thermogravimetric analysis (TGA, Swiss Mettler) using N_2 as the purge gas. X-ray photoelectron spectroscopy (XPS) was performed on an X-ray photoelectron spectroscope (Thermo Scientific K-Alpha, America), and all binding energies were calibrated using the C 1s peak (284.8 eV). Zeta potential measurement (Zetasizer Nano-ZS90, Malvern Instruments, UK) was carried out to analyze the surface charge of the catalyst at different pH values. Additionally, Raman spectra (Horiba, Japan) was conducted to assess the defect degree of the samples. Inductively coupled plasma atomic emission spectroscopy (ICP−MS, Agilent 7800, USA) was used to detect the concentration of metal ions leached during the reaction.

Text S5. Analysis of in situ Raman

The surface chemical changes of the CoNiFc-MOF catalyst during PDS activation were investigated by laser confocal Raman spectroscopy (Horiba, Japan). In detail, 5 mg of the CoNiFc-

MOF catalyst was deposited onto a glass slide and compressed into a sheet approximately 1 mm thick. The slice was then treated with a PDS solution (2 mM) and BPA solution, if needed) followed by scanning in the range of 300-1200 cm^{-1}. The same procedure was conducted with a PDS solution in the absence of catalyst.

Text S6. EPR measurements, experimental analysis of N_2 purge and exploration of high-value metal species

The signals of active radicals were investigated by electron paramagnetic resonance (EPR, Bruker EMXplus-6/1). Sulfate radical ($SO_4^{\bullet-}$) and hydroxyl radical ($^{\bullet}OH$) in solution were detected in solution by using 5,5-dimethyl-1-pyrrolineN-oxide (DMPO) as spin trapping agent, while singlet oxygen ($^1O_2$) was detected using 2,2,6,6-tetramethyl-4-piperidinol (TEMP). The detection of superoxide radical ($O_2^{\bullet-}$) followed a similar procedure to ($SO_4^{\bullet-}$), with the exception of using pure methanol as the solvent. To initiate the reactions,10 mg CoNiFc-MOF, 0.2 mM PDS, and 10 mg/L BPA solutions were utilized. A sample concentration of 1 mg/mL in deionized water or methanol was ultrasonically dispersed for 1 min. Subsequently, 30 μL of sample was mixed with 50 μL of DMPO (100 mM deionized water / methanol as solvent), and the resulting mixture was placed in a capillary tube within a quartz tube for EPR analysis of $^{\bullet}OH$ and $SO_4^{\bullet-}$. The detection of $^1O_2$ followed the same procedure, replacing DMPO with TEMP.

Further examination of whether the BPA removal was affected under anaerobic conditions (continuous N_2 purge) revealed minimal variation in the removal rate, indicating a negligible role of dissolved oxygen in the generation of $O_2^{\bullet-}$ and $^1O_2$ (Fig. S14).

To assess the involvement of high-valent metal species in the degradation of BPA within the CoNiFc-MOF/PDS system, ethyl phenyl sulfoxide (PMSO) and dimethyl sulfoxide (DMSO) were utilized as probes to detect these species. The concentration of PMSO remained constant, and $PMSO_2$ was nearly undetectable (Fig. S15). Furthermore, increasing the DMSO concentrations from 10 mM to 20 mM, had minimal impact on BPA removal, indicating that the influence of high-valent metal species on BPA removal is likely negligible (Fig. S16).

Text S7. Electrochemical measurements and analytical details

All the electrochemical experiments were carried out using the (CHI 760E, China Aged) electrochemical workstation with a traditional three-electrode system. To prepare the CoNiFc-coated carbon paper electrode (CoNiFc-MOF@CP), carbon paper (CP) was cut into thin slices measuring 2 cm × 3 cm and cleaned thoroughly with Anhydrous ethanol and deionized water. A mixture of 200 mg CoNiFc-MOF in 4 mL Anhydrous ethanol, supplemented with 100 μL Nafion solution as polymer adhesive, was sonicated for30 min to achieve a homogenous suspension. This suspension was coated onto one side of the carbon paper and dried for 20 min. The process was repeated on the other side of the carbon paper to ensure an even distribution of the catalyst. The CoNiFc-MOF@CP catalyst served as working electrode, while Ag/AgCl and platinum electrodes were used as reference electrode and counter electrodes, respectively. Electrochemical impedance spectroscopy (EIS), linear sweep voltammetry (LSV), chronoamperometry (I-t) and open circuit potential (OCP) analysis were performed in a 0.3 M Na_2SO_4 electrolyte solution.

The surface charge transfer capability of the CoNiFc-MOF, CoFc-MOF and NiFc-MOF composites was evaluated by electrochemical impedance spectroscopy (EIS). The analysis revealed that CoNiFc-MOF demonstrated a smaller charge transfer resistance (161.5 Ω) compared to CoFc-MOF (348.6 Ω) and NiFc-MOF (333.5 Ω) (Fig. S18 (a)). These findings suggest that the CoNiFc-MOF catalyst possesses superior interfacial electron transfer capabilities, which facilitate the rapid activation of PDS and enhance catalytic activity. The LSV curves for different catalysts were analyzed, as detailed in Fig. S18 (b). Furthermore, the observed current variations follow the trend : CoNiFc-MOF＞CoFc-MOF＞NiFc-MOF, consistent with the removal efficiency trend of BPA. The extent of current variation followed the trend: CoNiFc-MOF > CoFc-MOF > NiFc-MOF, which aligns with the observed trend in BPA removal efficiency.

Text S8. HPLC-MS operation

The degradation intermediates of BPA were identified using HPLC-MS (Thermo Scientific, USA). Eluent A consisted of water with 0.1% formic acid, while eluent B was acetonitrile. Elution was performed at a flow rate of 500 μL/min, with a column temperature of 40°C and the injection volume was 20 μL. The gradient elution program was as follows: 0-1 min, 10% acetonitrile; 9-14 min, 10-90% acetonitrile; 16-20 min, 90% acetonitrile. Further analysis of the m/z and molecular structure of the potential intermediates was conducted out using MS software, with the intermediate product details provided in Table S2.

Text S9. XPS analysis of different catalyst

The high-resolution Co 2p XPS spectra of CoFc-MOF and CoNiFc-MOF are shown in Fig. S9 (b). The presence of Co^{2+} in the XPS spectrum of Co 2p was identified by the existence of the main peaks at 781.0 eV and 797.3 eV, representing the Co $2p_{3/2}$ and Co $2p_{1/2}$ binding energies, respectively.[1] Furthermore, characteristic satellite peaks at 785.9 and 802.7 eV were observed, representing typical features of Co^{2+} in CoFc-MOF[2]. Upon the introduction of Ni^{2+} into CoFc-MOF, a slight shift towards lower binding energy was observed in the XPS peak position of Co^{2+} in CoNiFc-MOF ($2p_{3/2}$ was 780.9 eV), indicating partial migration of valence electrons and electron gain by Co. The XPS binding energy of Fe species in CoNiFc-MOF exceeds that in NiFc-MOF and CoFc-MOF (Fig.S9(c)), indicated partial electron transfer from Fc groups to the metal center, with most irons exiting as Fe^{2+}[2]. Similarly, the binding energy of Fe 2p shift towards higher binding energy (708.1 and 720.9 eV), indicating electron loss for Fe. The Ni 2p XPS spectra of NiFc-MOF are shown in Fig. S9 (d), with Ni^{2+} being identified by the main peaks at 855.9 eV and873.2 eV for the Ni $2p_{3/2}$ and Ni $2p_{1/2}$ spin orbits, along with respective satellite peaks at 860.8 eV and 879.8 eV[2].With the addition of Co^{2+}, the XPS peak of CoNiFc-MOF slightly shifted towards higher binding energy (860 and 873.5 eV for $2p_{3/2}$ and $2p_{1/2}$; 861.6 and 879.9 eV for satellite peaks), indicating partial movements of valence electrons and a minor electron loss for Ni. Collectively, the XPS results support the notion that the transition metal facilitates directional charge transfer, consequently enhancing the catalytic activity of CoNiFc-MOF.

Part S2. Supplementary Figures

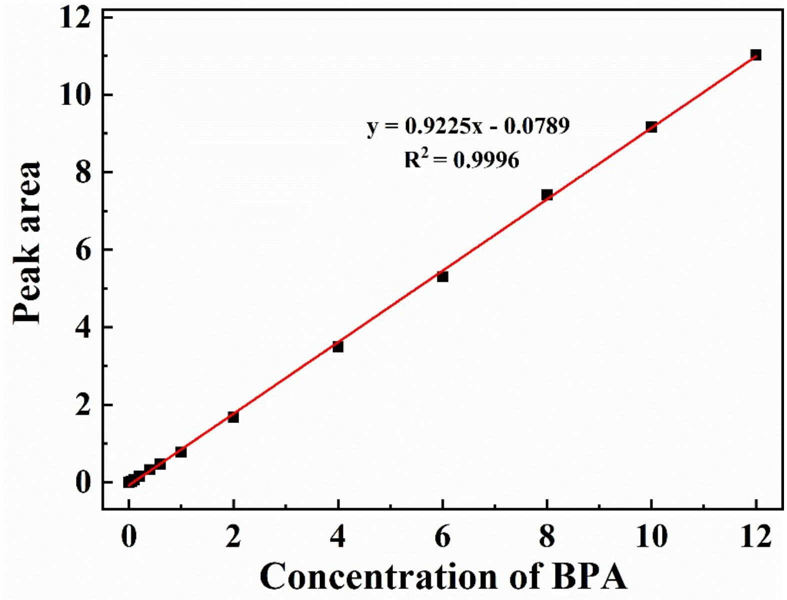

Fig. S1. BPA Standard Curve

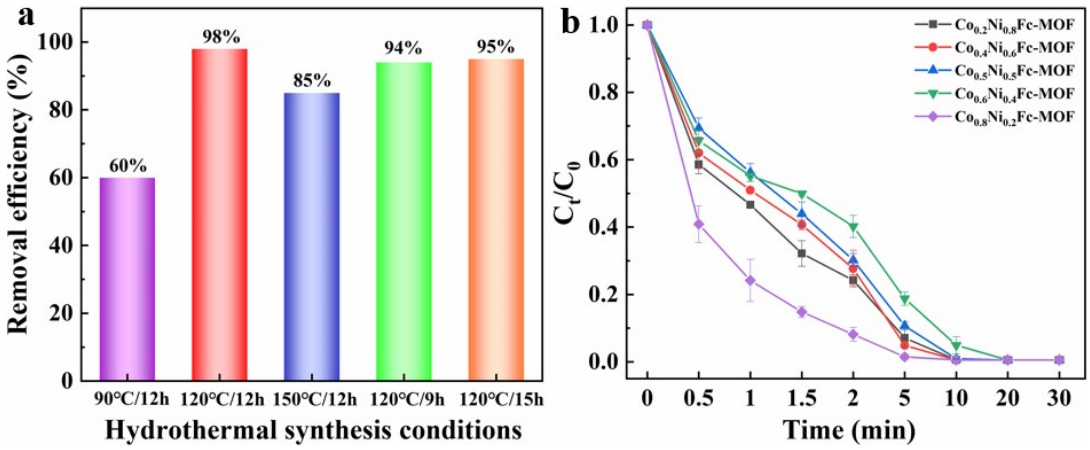

Fig. S2. (a) The effect of different reaction temperatures and times on the synthesis of CoNiFc-MOF catalyst for BPA removal. (b) The effect of different metal source ratios on the synthesis of CoNiFc-MOF catalyst for BPA removal. Experimental condition; catalysts = 10 mg; PDS = 200 μM; pH = 8.2 (initial pH unadjusted);T=25°C.

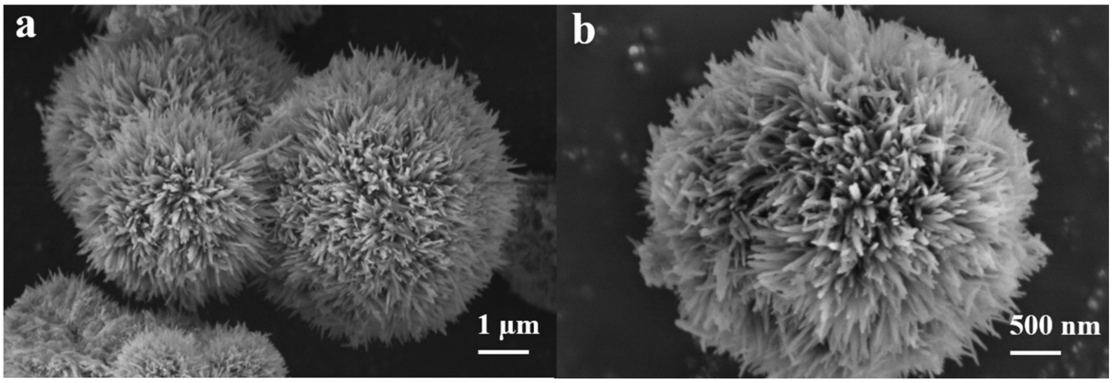

Fig. S3. SEM images of the CoFc-MOF (a-b)

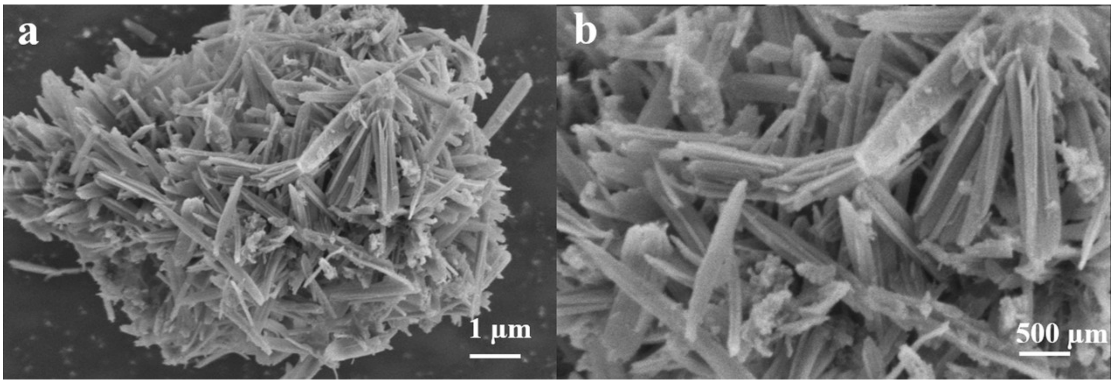

Fig. S4. (a-b) SEM images of the NiFc-MOF.

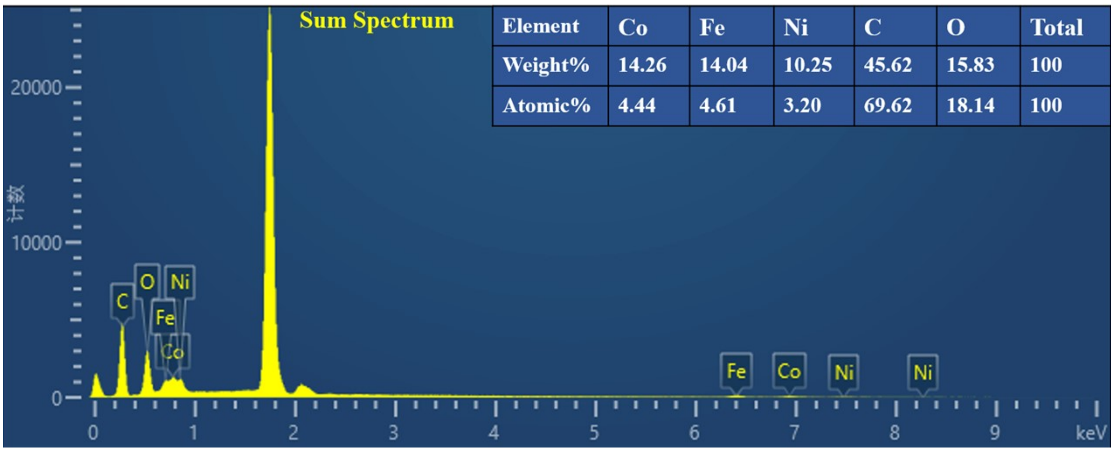

Element	Co	Fe	Ni	C	O	Total
Weight%	14.26	14.04	10.25	45.62	15.83	100
Atomic%	4.44	4.61	3.20	69.62	18.14	100

Fig. S5. EDS spectrum of CoNiFc-MOF.

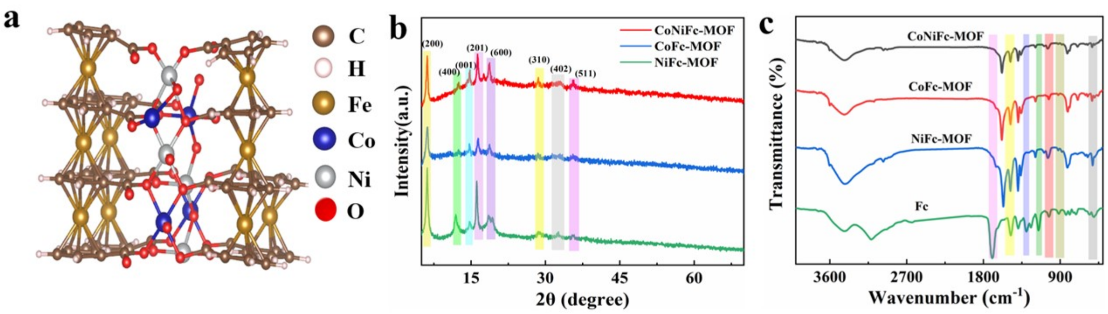

Fig. S6. (a) The crystal structure of CoNiFc-MOF (lattice parameters a = 20.12 Å, b = 7.09 Å, c = 30.59 Å, α=90° β= 90°， γ=88.72°, V= 593.5 Å3); (b) Characterization images of different catalysts: XRD patterns; (c) FT-IR spectra.

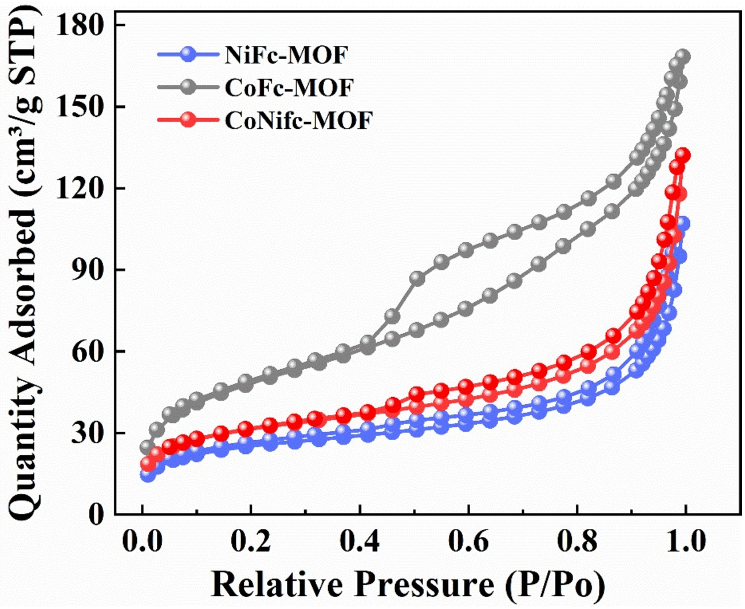

Fig. S7. N_2 adsorption-desorption isotherms of NiFc-MOF, CoFc-MOF and CoNiFc-MOF catalysts.

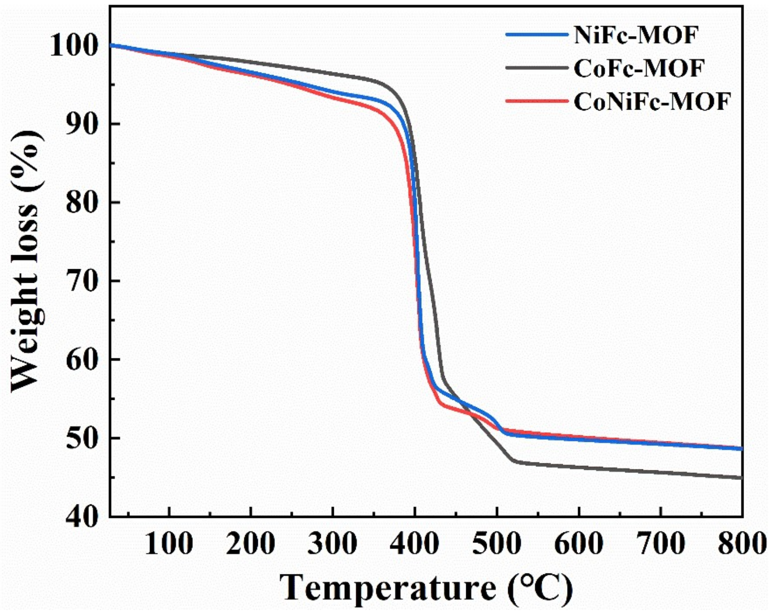

Fig.S8. Thermal Gravimetric Curves of NiFc-MOF, CoFc-MOF and CoNiFc-MOF Catalysts.

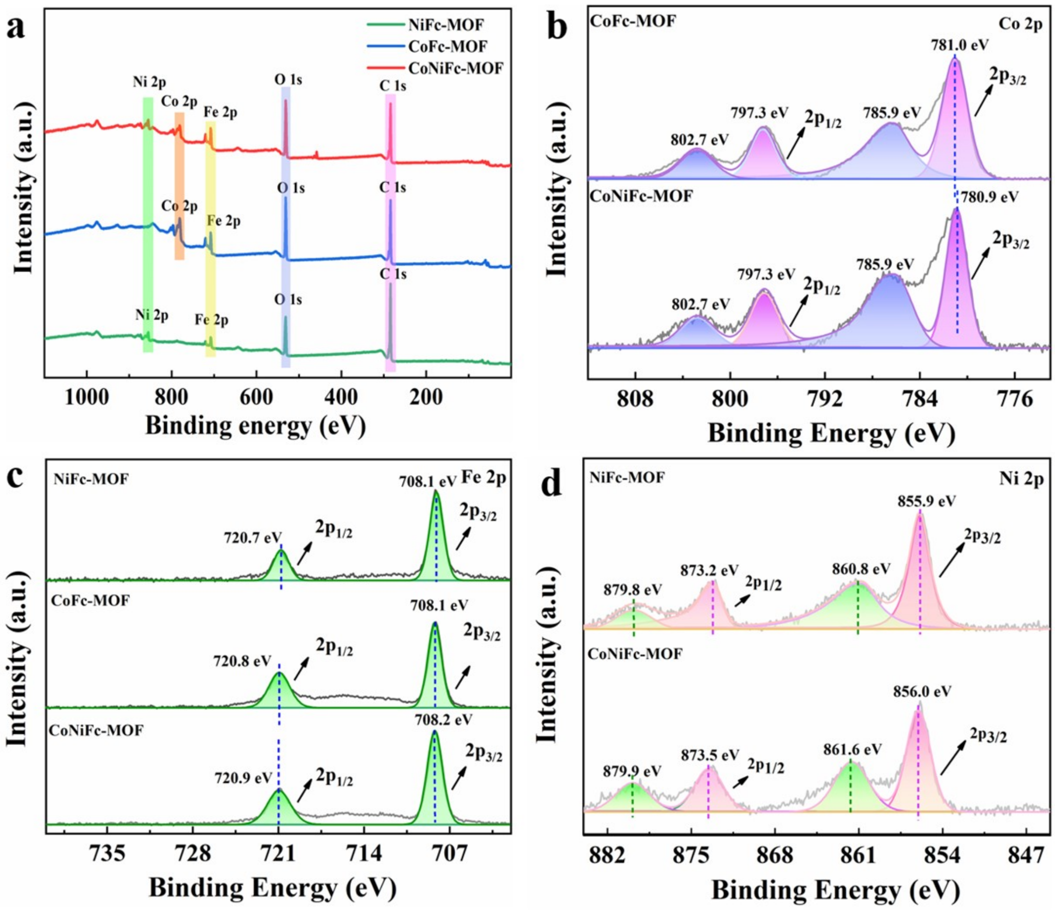

Fig. S9. (a) XPS survey of CoNiFc-MOF. High resolution XPS spectra of (b) Co 2p, (c) Fe 2p, (d) Ni 2p of catalysts.

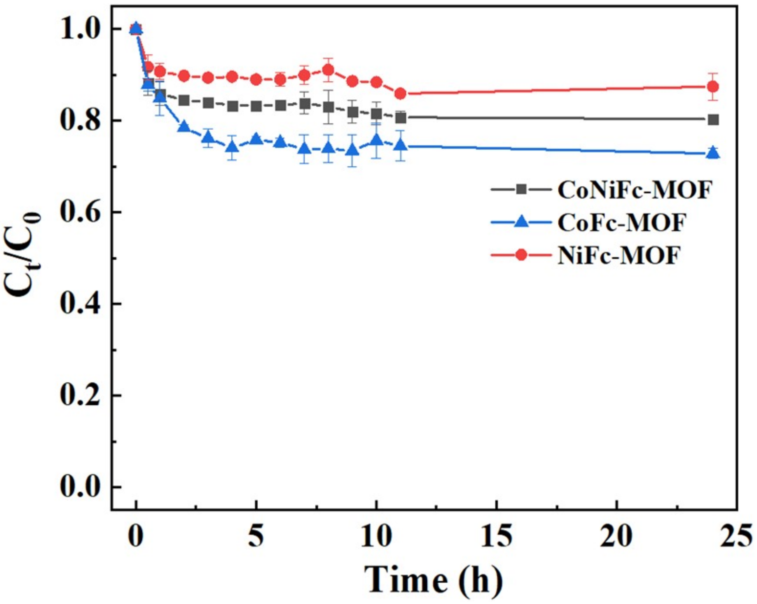

Fig. S10. Adsorption of BPA by NiFc-MOF, CoFc-MOF and CoNiFc-MOF catalysts. Experimental condition; catalysts = 10 mg; PDS = 200 µM; pH = 8.2 (initial pH unadjusted); T=25°C;

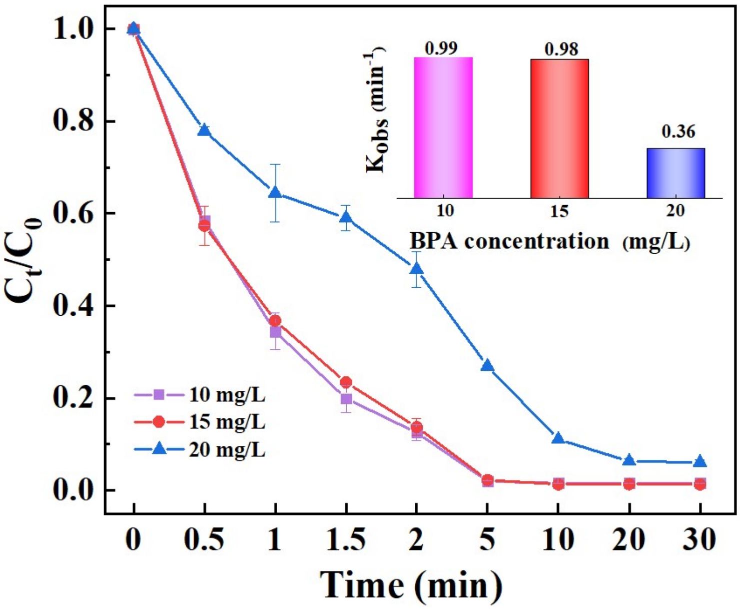

Fig. S11. Effects of different BPA concentrations on degradation. Experimental condition; catalysts = 10 mg; PDS = 200 μM; pH = 8.2 (initial pH unadjusted); T=25℃;

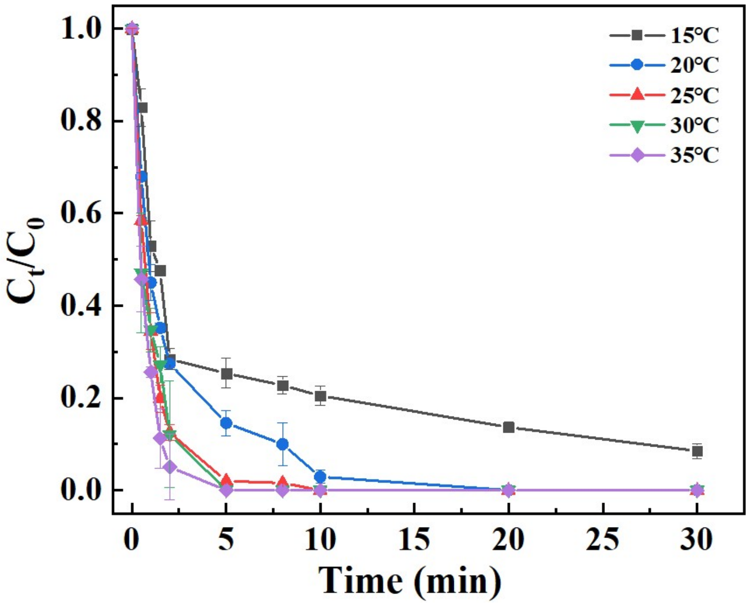

Fig. S12. Effect of different temperatures on BPA removal. Experimental condition; catalysts = 10 mg; PDS = 200 μM; pH = 8.2 (initial pH unadjusted); T=25℃;

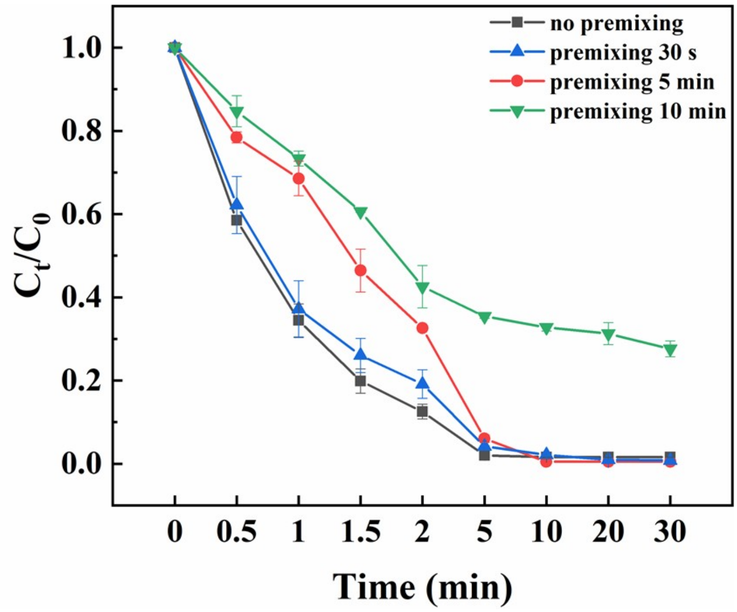

Fig. S13. Premixing CoNiFc-MOF and PDS on BPA degradation. Experimental condition: BPA = 10 mg/L; catalysts = 10 mg; PDS = 200 μM; pH = 8.2 (initial pH unadjusted); T=25°C;

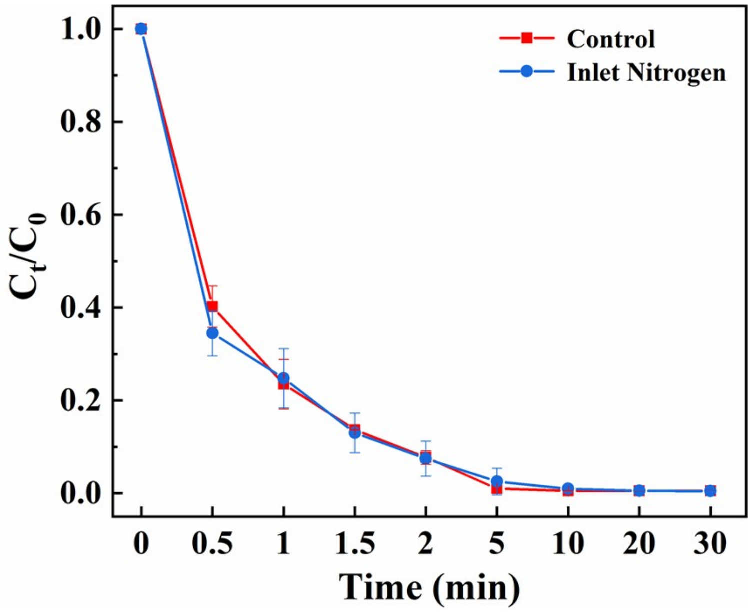

Fig. S14. BPA degradation in CoNiFc-MOF/PDS system with or without N_2 bubbling. Reaction conditions: BPA = 10 mg/L; catalysts = 10 mg; PDS = 200 μM; pH = 8.2 (initial pH unadjusted); T=25°C;

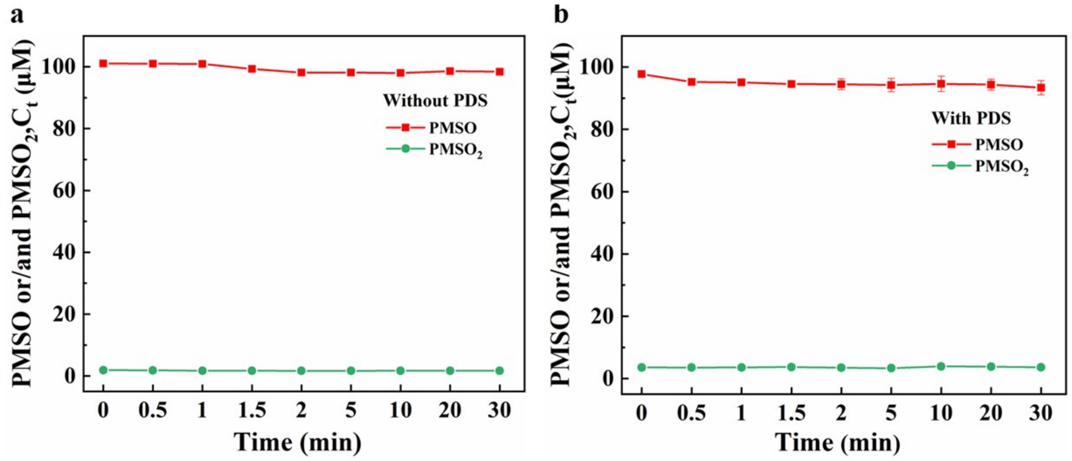

Fig. S15. (a) PMSO consumption and PMSO$_2$ generation in in different systems: CoNiFc-MOF alone system. (b) CoNiFc-MOF/PDS system. Experimental condition: BPA = 10 mg/L; catalysts = 10 mg; PDS = 200 μM; pH = 8.2 (initial pH unadjusted); T=25°C;

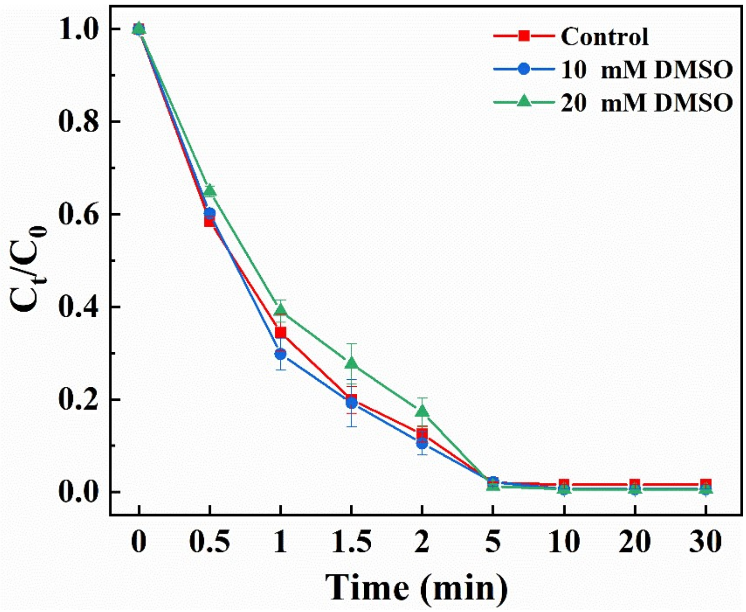

Fig. S16. Effect of DMSO on BPA degradation in the CoNiFc-MOF/PDS system. Experimental condition: BPA = 10 mg/L; catalysts = 10 mg; PDS = 200 μM; pH = 8.2 (initial pH unadjusted); T=25°C;

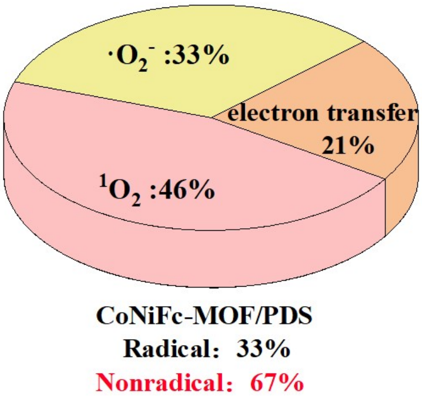

Fig. S17. ROS contribution of CoNiFc-MOF/PDS system.

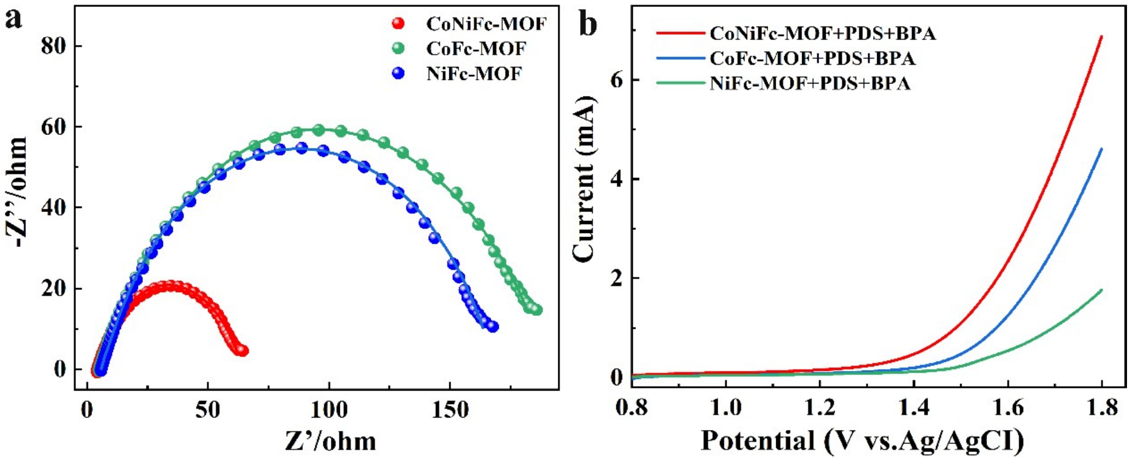

Fig. S18. Electrochemical impedance spectroscopy (EIS) analysis of CoNiFc-MOF, CoFc-MOF and NiFc-MOF samples (a); LSV results of CoNiFc-MOF, CoFc-MOF and NiFc-MOF (b). Experimental condition: catalysts = 10 mg, BPA = 10 mg/L; PDS = 200 µM, Na_2SO_4=0.3 M.

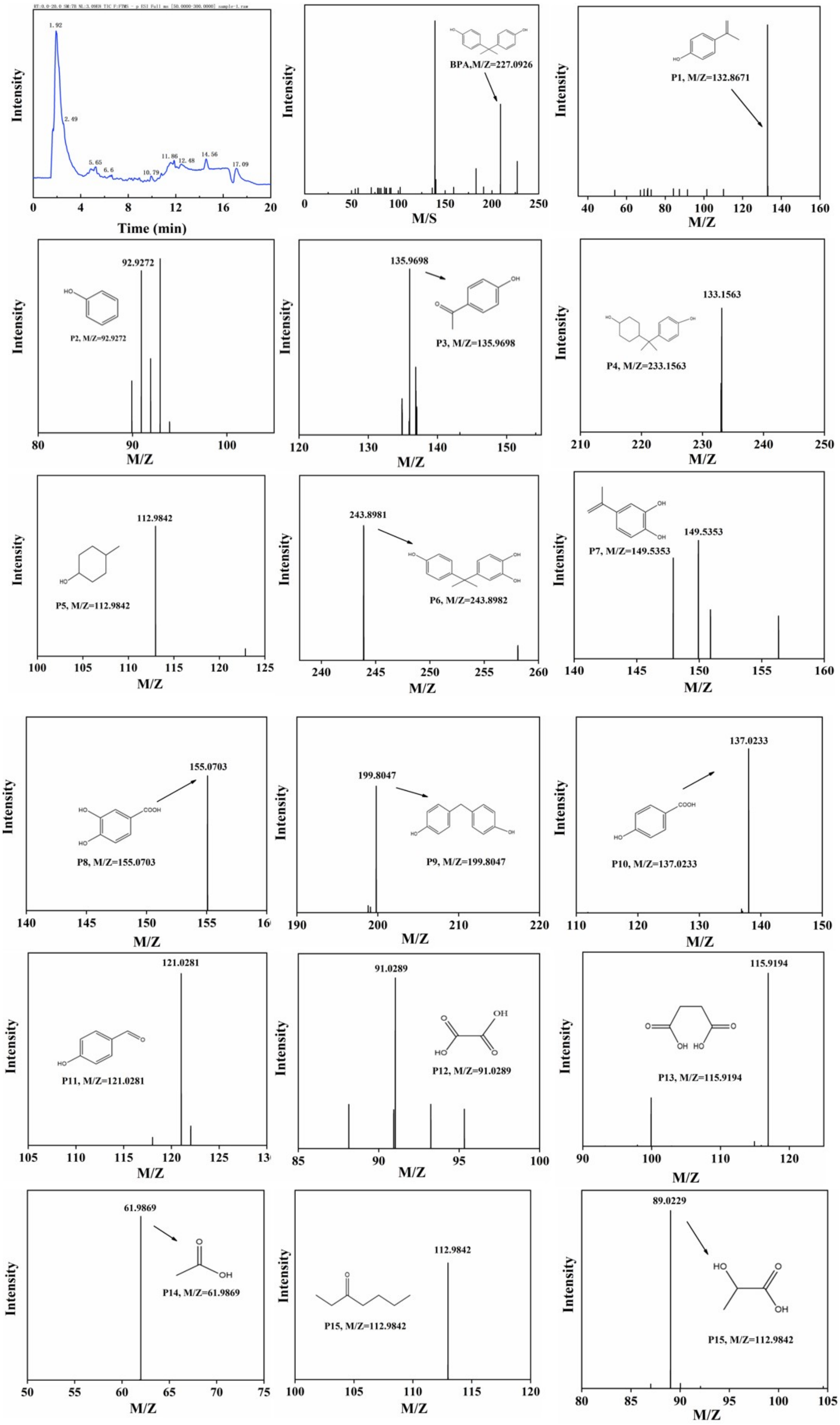

Fig. S19. MS spectra of the BPA intermediates detected in the CoNiFc-MOF/PDS system.

Part S3. Supplementary Tables

Table S1. The HPLC analysis conditions for different organic compounds.

Compound	Mobile phase	Ratio (V/V)	Wavelength nm	Column temperature	Flow rate (mL/min)
BPA	CH_3OH: H_2O	70:30	208	40℃	0.8
BPB	CH_3OH: H_2O (1% formic acid)	80:20	268	30℃	0.8
TC	CH_3OH: $C_2H_2O_4$	30:70	280	35℃	0.8
OTC	C_2H_3N: H_2O (1% formic acid)	20:80	264	35℃	0.8
PE	C_2H_3N: H_2O (1% formic acid)	40:60	270	30℃	1
PMSO	C_2H_3N: H_2O	30:70	230	35℃	1
$PMSO_2$	C_2H_3N: H_2O	30:70	215	35℃	1

Table S2. Relative element content (wt.%) on catalyst surface.

Catalyst	**Relative content (wt.%)**				
	O 1s	**C 1s**	**Fe 2p**	**Co 2p**	**Ni 2p**
CoNiFc-MOF before reaction	26.76	62.19	4.54	4.03	2.49
CoNiFc-MOF after reaction	27.98	62.11	4.39	3.29	2.23

Table S3. The changes in the content of elemental valence states before and after the CoNiFc-MOF reaction.

Catalyst	**Oxidation state ratio (%)**					
	Fe^{2+}	**Fe^{3+}**	**Co^{2+}**	**Co^{3+}**	**Ni^{2+}**	**Ni^{3+}**
Feresh	100%	0%	47.33%	0%	65.17	0%
Used	59.58%	40.42%	49.91%	0%	44.38	0%
change	-59.58%	+40.42%	+2.58	0%	-21.79	0%

Table S4. The identified intermediates of BPA by UPLC-Q-TOF-MS in the CoNiFc-MOF/PDS system.

Products	RT (min)	MFG formula	m/z $[M\text{-}H]^-$	Structure
BPA	6.98	$C_{15}H_{15}O_2$	227.09261	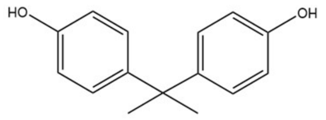
P1	18.49	$C_9H_{10}O$	132.86711	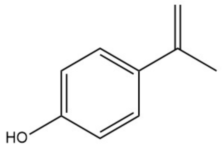
P2	16.91	C_6H_6O	92.92723	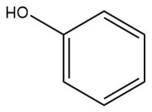
P3	13.36	$C_8H_8O_2$	135.96977	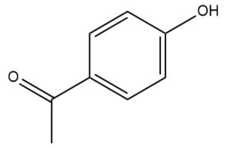
P4	5.83	$C_{15}H_{22}O_2$	233.15625	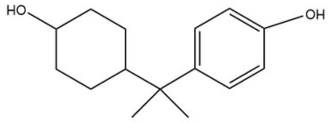
P5	4.25	$C_7H_{14}O$	112.9842	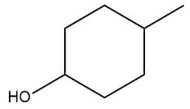
P6	16.91	$C_{15}H_{16}O_3$	243.89812	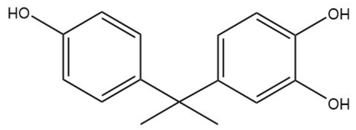
P7	1.73	$C_8H_{10}O_2$	149.5353	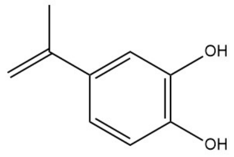
P8	7.76	$C_7H_6O_4$	155.07029	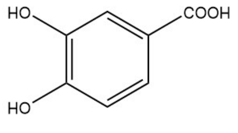

P9	6.91	$C_{13}H_{12}O_2$	199.8047	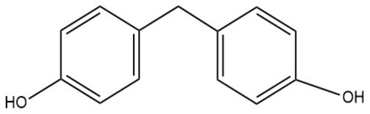
P10	7.46	$C_7H_6O_3$	137.0233	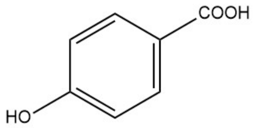
P11	5.53	$C_7H_6O_2$	121.02813	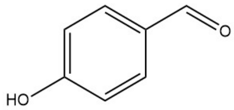
P12	16.9	$C_2H_2O_4$	91.0289	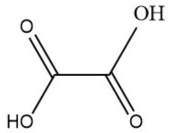
P13	16.08	$C_4H_6O_4$	115.9194	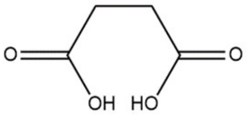
P14	0.40	$C_2H_4O_2$	61.98687	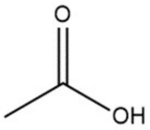
P15	4.25	$C_7H_{14}O$	112.9842	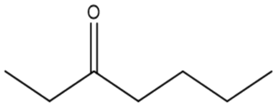
P16	2.50	$C_3H_6O_3$	89.02291	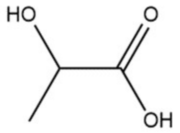

Table S5. Calculate the percentage ratio of different metals leaching

Metal	**Initial Catalyst Content (mg/g)**	**Solution Concentration (mg/L)**	**Solution Volume (L)**	**Leached Mass (mg)**	**Leaching Percentage (%)**
Co	154.8	1.9	0.05	0.095	3.9%
Fe	126.9	1.2	0.05	0.060	7.5%
Ni	17.2	1.3	0.05	0.065	3.8%

Table S6. The comparison of recently reported transition metal catalysts in PMS/PDS activation for the removal of BPA.

Catalysts	Dosage (g/L)	PDS[a]/PMS[b] (mM)	C_{BPA} (mg/L)	pH	Removal efficiency	Ref.
Fe-MOF/BN	0.15	1[b]	20	7.0	93.3% (90 min)	[3]
FeMn-350	0.5	0.65[b]	80	7.5	100% (30 min)	[4]
$CuFe_2O_4$–Fe_2O_3	0.2	1.17[b]	5	7.2	100% (10 min)	[5]
$Fe_1Mn_5Co_4$-N@C	0.1	0.2[b]	20	6.0	100% (10 min)	[6]
$Mn_{0.27}FeO_{4.55}$	0.5	2[a]	10	7.3	97.8% (90 min)	[7]
Fe/Mn@NBC_{800}	0.2	3[b]	20	6.85	100% (20 min)	[8]
Zn-OMS-2	0.25	2[a]	20	7	58.4% (35 min)	[9]
NiO-12	0.1	0.2[b]	20	7.9	100% (20 min)	[10]
CoNiFc-MOF	0.01	0.2[b]	10	8.2	98% (5 min)	This work

References

1. Q. Mo, H. Zheng and G. Sheng, A heterogeneously activated peroxymonosulfate with a Co and Cu codoped bimetallic metal-organic framework efficiently degrades tetracycline in water, *Molecular Catalysis*, 2024, **553**, 113817.
2. J. Hu, Q. Xu, X. Wang, X. Huang, C. Zhou, Y. Ye, L. Zhang and H. Pang, Charge‐transfer‐regulated bimetal ferrocene‐based organic frameworks for promoting electrocatalytic oxygen evolution, *Carbon Energy*, 2023, **5**, 1-12.
3. Y. Wan, W. Zhang, X. Han, L. Zhou, H. Zhen, C. Wu, Q. Yu and G. Xiu, B,N-decorated carbocatalyst based on Fe-MOF/BN as an efficient peroxymonosulfate activator for bisphenol A degradation, *J. Hazard. Mater.*, 2022, **430**, 127832.
4. L. Yu, G. Zhang, C. Liu, H. Lan, H. Liu and J. Qu, Interface Stabilization of Undercoordinated Iron Centers on Manganese Oxides for Nature-Inspired Peroxide Activation, *ACS Catalysis* 2018, **8**, 1090-1096.
5. W. Oh, Z. Dong, Z. Hu and T. Lim, A novel quasi-cubic $CuFe_2O_4$–Fe_2O_3 catalyst prepared at low temperature for enhanced oxidation of bisphenol A via peroxymonosulfate activation, *J. Mater. Chem. A*, 2015, **3**, 22208-22217.
6. X. Li, Z. Ao, J. Liu, H. Sun, A. I. Rykov and J. Wang, Topotactic Transformation of Metal–Organic Frameworks to Graphene-Encapsulated Transition-Metal Nitrides as Efficient Fenton-like Catalysts, *ACS Nano*, 2016, **10**, 11532-11540.
7. Y. Ma, D. Wang, Y. Xu and H. Lin, Nonradical electron transfer-based peroxydisulfate activation by a Mn−Fe bimetallic oxide derived from spent alkaline battery for the oxidation of bisphenol A, *J. Hazard. Mater.*, 2022, **436**, 129172.
8. Z. Zhang, H. Ding, Y. Li, J. Yu, L. Ding, Y. Kong and J. Ma, Nitrogen-doped biochar encapsulated Fe/Mn nanoparticles as cost-effective catalysts for heterogeneous activation of peroxymonosulfate towards the degradation of bisphenol-A: Mechanism insight and performance assessment, *Sep. Purif. Technol*, 2022, **283**, 120136.
9. J. Li, Z. Hao, J. Jin, C. Fang, Z. Yang, X. Meng and X. Liu, Facile synthesis of Zn-OMS-2 nanorods for enhanced degradation of bisphenol A via PDS activation, *Inorg. Chem. Commun.*, 2023, **153**, 110791.
10. L. Zhou, P. Liu, Y. Ding, J. Xi, L. Liu, W. Wang and J. Xu, Hierarchically porous structure of two-

dimensional nano-flakes assembled flower-like NiO promotes the formation of surface-activated complex during persulfate activation, *Chem. Eng. J.*, 2022, **430**, 133134.